ACS APPLIED MATERIALS & INTERFACES

Research Article

www.acsami.org

Highly Efficient Photocatalytic Performance of Graphene–ZnO Quasi-Shell–Core Composite Material

Yuyu Bu,[†] Zhuoyuan Chen,*[,†] Weibing Li,[‡] and Baorong Hou[†]

[†]Key Laboratory of Marine Environmental Corrosion and Bio-fouling, Institute of Oceanology, Chinese Academy of Sciences, 7 Nanhai Road, Qingdao 266071, China

[‡]School of Environment and Safety Engineering, Qingdao University of Science and Technology, 53 Zhengzhou Road, Qingdao 266042, China

ABSTRACT: In the present paper, the graphene–ZnO composite with quasi-shell–core structure was successfully prepared using a one-step wet chemical method. The photocatalytic Rhodamine B degradation property and the photoelectrochemical performance of the graphene–ZnO quasi-shell–core composite are dependent on the amount of graphene oxide that is added. When the amount of graphene oxide added is 10 mg, the graphene–ZnO quasi-shell–core composite possesses the optimal photocatalytic degradation efficiency and the best photoelectrochemical performance. An efficient interfacial electric field is established on the interface between the graphene and ZnO, which significantly improves the separation efficiency of the photogenerated electron–hole pairs and thus dramatically increases its photoelectrochemical performance. In addition to the excellent photocatalytic and photoelectrochemical properties, the electron migration ability of the grephene–ZnO quasi-shell–core composite is significantly enhanced due to the graphene coating on ZnO surface; therefore, this material has great potential for application as a substrate material to accept electrons in dye solar cell and in narrow bandgap semiconductor quantum dot sensitized solar cells.

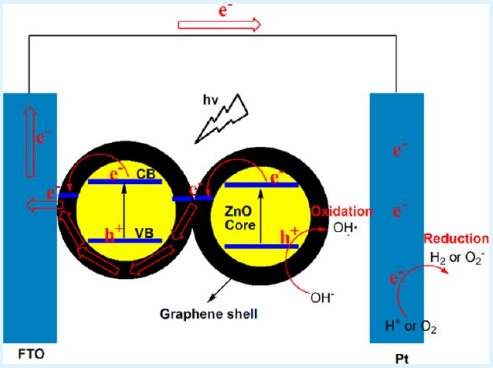

KEYWORDS: *graphene, ZnO, quasi-shell–core, photocatalysis, photoelectrochemistry*

1. INTRODUCTION

In recent years, the application of graphene–inorganic semiconductor composite materials in the area of solar energy conversion has caused widespread concern in the research community.[1−3] Graphene is a two-dimensional material composed of sp2-bonded carbon atoms that are linked in hexagonal shapes, with each carbon atom covalently bonded to three other carbon atoms. Graphene possesses very high charge carrier mobility and specific surface area, and these properties can significantly improve the separation efficiency of photogenerated electron–hole pairs and increase the reaction active sites during a photocatalytic process. Furthermore, a strong heterojunction electric field is formed on the interface between graphene and an inorganic semiconductor material due to the difference in their Fermi levels. Photogenerated electrons are swiftly transferred to the surface of graphene and participate in the reduction reactions occurring there, significantly enhancing the separation efficiency of photogenerated electron–hole pairs and the photocatalytic ability. Therefore, graphene composite photocatalysts should be developed and their application in the areas of photocatalysis and photoelectrochemistry should be investigated.

It has been reported that large-area monodispersed graphene, loaded with inorganic semiconductor materials, such as TiO_2,[4−6] ZnO,[7,8] CdS,[9,10] $BiVO_4$,[11,12] $ZnFe_2O_4$,[13] etc., shows significantly improved photocatalytic performance. Under illumination, the electrons generated in the inorganic semiconductor materials can be swiftly transferred to the graphene through the interface between these two materials and participate in reduction reactions occurring on graphene surface. Meanwhile, photogenerated holes remain on the surface of the inorganic semiconductor materials and participate in oxidation reactions occurring on their surfaces. However, it is worth noting that the contact area between graphene and the inorganic semiconductor materials is relatively small and the effective area of the heterojunction electric field built on the interface is low using this complex method.[1] Thus, it cannot achieve optimum photocatalytic performance. Recently, Kim et al.[14] obtained small pieces of graphene oxide (GO) by breaking GO with large piece structures. These small pieces of GO were then successfully loaded onto the surfaces of TiO_2 nanoparticles and subsequently reduced to form graphene by photoassisted reduction. Their investigations showed that the photoelectrochemistry and photocatalytic water reduction performance of the small pieces of graphene-coated TiO_2 nanocomposite materials are clearly improved when compared with those of large pieces of graphene-coated TiO_2 nanocomposite materials. The performance improvement is

Received: July 31, 2013
Accepted: November 9, 2013
Published: November 9, 2013

attributed to a three-dimensional nanocoating structure, due to TiO_2 being completely coated and in close contact with graphene. This type of structure can increase the separation efficiency of photogenerated electron−hole pairs and the migration rates of photogenerated electrons and holes, resulting in an increase in the lifetime of the charge carriers. Therefore, this graphene-coated photocatalyst is more attractive than a photocatalyst on which graphene is directly loaded.

Zinc oxide (ZnO) is a semiconductor material with a wide bandgap, which is responsive to ultraviolet light. Because it is inexpensive and environmentally friendly and it possesses strong photoinduced hole oxidation ability, ZnO has been widely studied for its use in solar cell,[15,16] photocatalytic hydrogen production from water splitting,[17−19] photocatalytic degradation of organic pollutants,[20−24] photoluminescence,[25] etc. In addition, the electron mobility in ZnO is approximately two orders of magnitude higher than that in TiO_2. This higher electron mobility can effectively improve the migration rate of photogenerated electrons in ZnO and inhibit the recombination of photogenerated electrons and holes, and can hence increase the lifetime of the photogenerated charge carriers. Therefore, ZnO is considered as a photovoltaic semiconductor material with significant application potential.

Recently, Son et al.[26] prepared graphene-coated ZnO quasi-shell−core structure materials by a one-step heating reaction method using graphite oxide and zinc acetate as raw materials. The composite material was studied in the application in a light-emitting diode and achieved excellent results. However, to the best of our knowledge, there have been few studies investigating the photocatalytic and photoelectrochemical properties of similar materials including the effect of the graphene and ZnO composite ratio related to the above properties. Therefore, in consideration of the potential applications of this new type of nanostructure based on the promotion of the photocatalytic and photoelectrochemical properties, the authors prepared graphene−ZnO composite materials with a quasi-shell−core structure and further optimized its photoelectrochemical properties and its photocatalytic Rhodamine B (RhB) degradation performance. The mechanism of the related performance improvement was also analyzed in this work.

2. EXPERIMENTAL SECTION

2.1. Preparation of the Graphene−ZnO Quasi-Shell−Core Composite Materials. A certain amount of GO (3, 5, 10, 20, and 40 mg), which was prepared based on the method used by Hummers et al.,[27] was dispersed in 40 mL dimethylformamide (DMF), and the resulting mixture was ultrasonically vibrated for 30 min. This dispersion liquid was subsequently added slowly to a $Zn(Ac)_2{\cdot}2H_2O$ DMF solution prepared by dissolving 0.92 g $Zn(Ac)_2{\cdot}2H_2O$ in 200 mL DMF under strong agitation. The liquid mixture was stirred for 5 h at 95 °C. After that, the liquid mixture was centrifugalized and the centrifugate was repeatedly washed with anhydrous ethanol. The graphene−ZnO quasi-shell−core composite materials with different GO addition were obtained after drying at 55 °C for 12 h under vacuum conditions. All reagents used in this study were analytical ones from Aladdin reagent corporation.

2.2. Characterizations of the Prepared Graphene−ZnO Quasi-Shell−Core Composite Materials. The morphologies and the microstructure of the synthetic products were analyzed using a field emission scanning electron microscope (FESEM) (S4800, Hitachi, Japan) and a high-resolution transmission electron microscope (HRTEM, FEI Tecnai G20, FEI Company, USA). The elemental compositions, the crystalline structures, and bonding information of the synthetic products were analyzed using an energy dispersive spectrometer (EDS, FEI Tecnai G20, FEI Company, USA), X-ray diffraction (XRD, D/MAX-2500/PC; Rigaku Co., Tokyo, Japan), and X-ray photoelectron spectroscopy (XPS, Axis Ultra, Kratos Analytical Ltd., England). The optical absorption properties were investigated using a UV−vis diffuse reflectance spectrophotometer (U-41000; HITACHI, Tokyo, Japan).

2.3. Photocatalytic Degradation of RhB. A 0.1 g portin of prepared photocatalysts was added to 100 mL RhB with a concentration of 10 $mg{\cdot}L^{-1}$ and stirred for 30 min in the dark. The light source was a 300 W Xe arc lamp (PLS-SXE300, Beijing Changtuo Co. Ltd., Beijing, China). The distance between the light source and the dye liquid level is 10 cm. The temperature of the dye liquid was maintained at 25 °C using circulating water. The stability of the photocatalytic degradation in a graphene−ZnO composite with 10 mg of added GO was studied. The photocatalyst was recycled by the centrifugation of the solution after dye degradation and the centrifugate was used for the next cycle of RhB degradation after sufficient drying. Photocatalyst recycling tests were performed five times in this work.

2.4. Photoelectrode Preparation. An FTO glass (13 mm × 10 mm) was first ultrasonically cleaned with acetone of analytical grade for 5 min, rinsed with deionized water, and then dried with a clean, dry airflow. One longitudinal edge of the conductive side was then carefully covered with insulating tape, with the exposed effective area of the FTO glass measuring 1 cm^2. In total, 0.01 g of the prepared powder was mixed with 0.1 mL of deionized water in an agate mortar, and the mixture was carefully ground for 10 min to form a homogeneous suspension. Then, 0.025 mL of the as-prepared suspension was evenly distributed onto the exposed area of the conductive side of the FTO glass. The insulating tape on the edge of the FTO glass was removed after the suspension had dried in the air. Finally, the FTO glass deposited with the as-prepared suspension was heated to 120 °C for 2 h under vacuum condition. A copper wire was connected to the conductive side of the FTO glass using conductive silver tape. Uncoated parts of the conductive side of the FTO glass were isolated with parafilm after the conductive silver tape had dried.

2.5. Photoelectrochemical Measurements. Photoelectrochemical measurements were performed in a three-electrode experimental system using CHI660D Electrochemical Workstation (Shanghai Chenhua Instrument Co., Ltd., Shanghai, China). The prepared series photoelectrodes, saturated calomel electrode (SCE), and Pt electrode acted as the working, reference, and counter electrodes, respectively. The potentials are reported on the SCE scale. The photo, generated by a 150 W Xe arc lamp (PLS-SXE300, Beijing Changtuo Co. Ltd., Beijing, China), passed through a flat circular quartz window, equipped on the side of the three-electrode cell, and illuminated on the backside of the photoelectrode with an optical intensity of 265 mW cm^{-2}. The variations of the photoinduced current density with time (i−t curve) were measured at a 0 V bias potential (vs SCE) during 3-cycle light on and off. The photoinduced voltage−current (i−V) curves were measured from −0.8 to 1.0 V with a scan rate of 10 mV s^{-1}. The gap between the switching on and turning off of the light was 1 s. EIS tests were performed under dark condition at open circuit potential over the frequency range between 10^5 and 10^{-1} Hz, with an AC voltage magnitude of 5 mV, using 12 points/decade. All of the measurements were performed in 0.1 M Na_2SO_4 solution at ambient temperature.

3. RESULTS AND DISCUSSION

Figure 1 shows the scanning electron microscope (SEM) images of the ZnO and graphene−ZnO quasi-shell−core composite with different GO dosages (5, 10, and 20 mg). Figure 1a shows the SEM image of ZnO under low magnification, and Figure 1b shows that of ZnO under high magnification. ZnO exists as small nanoparticles and aggregates. The diameter of the aggregates is approximately 500 nm, as shown in Figure 1a. Figure 1b is the enlarged image of one of the aggregates and clearly shows that the aggregate is mainly

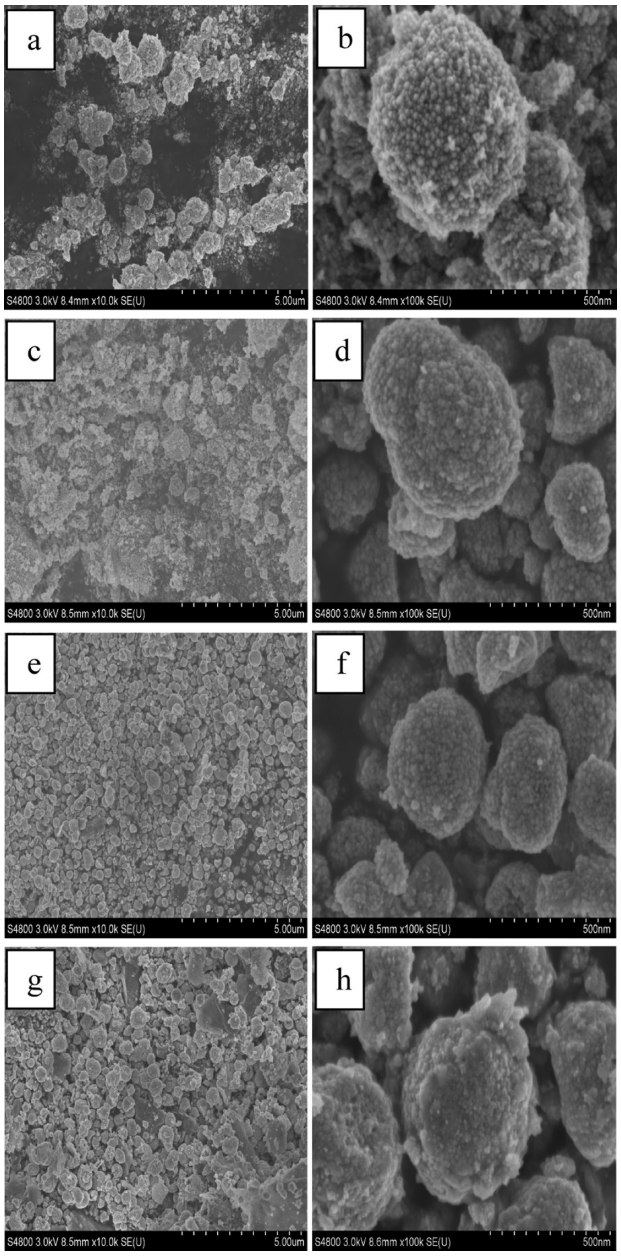

Figure 1. SEM images of the graphene−ZnO quasi-shell−core composite with different GO addition: (a, b) 0; (c, d) 5; (e, f) 10; (g, h) 20 mg.

formed by very small ZnO nanoparticles. Figure 1c and d shows the micromorphologies of the graphene−ZnO quasi-shell−core composite under both low and high magnification when the added GO in the reaction system is 5 mg. The micromorphology under low magnification is similar to that of ZnO shown in Figure 1a. However, under high magnification (Figure 1d), ZnO nanoparticles cannot be clearly observed in the ZnO aggregates and ZnO appears to combine more closely. When the added GO in the reaction system is increased to 10 mg, the composite is mainly composed of evenly distributed aggregates (Figure 1e), in contrast to the microstructure produced by the blending of very small nanoparticles with aggregates, as shown in Figure 1a and c. Under high magnification, the microstructure shown in Figure 1f is similar to that shown in Figure 1d. When the added GO in the reaction system increases to 20 mg, a large amount of laminar precipitations is clearly observed except for the larger aggregates under low magnification, as shown in Figure 1g. This result indicates that the added GO amount has exceeded the amount needed to cover all of the ZnO nanoparticles and a surplus is present. Under high magnification, a coating material layer is clearly observed on the surfaces of the aggregates and the ZnO nanoparticles are barely observed, as showed in Figure 1h. Therefore, through the above SEM results, graphene can completely coat all surfaces of ZnO nanoparticles and aggregates when the added GO amount is 10 mg. Higher GO additions will increase the thickness of the graphene coating layer and the surplus layer-structured graphene will be located between the ZnO aggregates.

In order to further study the graphene loading information on the ZnO surface, the composite with 10 mg adding GO was selected for HRTEM investigations. Figure 2a shows the microscopic morphology under low magnification. After ultrasonic dispersion, ZnO is found to exist in the form of evenly dispersed nanoparticles with size of approximately 15 nm. The ZnO aggregates, as shown in Figure 1b, are not observed after ultrasonic dispersion, indicating that ZnO in the aggregates has combined due to weak binding forces. Under high magnification, the ZnO (002) crystal plane is clearly observed and a coating layer approximately 1−2 nm thick covers the ZnO surface, as shown in Figure 2b. This result is similar to that obtained by Son et al.[26] The results indicate that 2−3 layers of graphene cover the surface of ZnO. Figure 2c shows the EDS results of the composite with 10 mg GO addition. Zn, O, C, and Cu elements are observed. The Cu element is observed because the EDS test was performed using HRTEM with a copper mesh substrate.

Figure 3 shows the XRD patterns of ZnO and the graphene−ZnO quasi-shell−core composite with different GO additions (5, 10, 20, and 40 mg). The crystal structure of the ZnO without graphene is similar to that of wurtzite, and the graphene coating does not affect the diffraction peaks of ZnO, revealing that graphene does not affect the crystal structure of ZnO. Graphene simply coats on the surface of ZnO, instead of doping into the ZnO crystal lattice. With an increase of the GO addition, a weak and broad diffraction peak appeared at 2θ = 25.8°, and the intensity of this peak increases with the GO addition. This diffraction peak is the characteristic index of the (002) crystal plane of graphene.[26]

X-ray photoelectron spectroscopy (XPS) was further used to investigate the states of zinc, oxygen, and carbon on the samples. Figure 4 shows the XPS spectra of the graphene−ZnO quasi-shell−core composite with 10 mg GO addition. Figure 4a shows the total survey spectrum. Figure 4b shows the Zn2p XPS core level spectrum. Binding energy peaks at 1021.68 and 1045.02 eV are observed, and these peaks are assigned to the electron orbits of $Zn_{2p3/2}$ and $Zn_{2p1/2}$.[7,8] Figure 4c shows the O1s XPS core level spectrum. Two binding energy peaks at 531.1 and 533.5 eV are obtained by curve fitting. The former one is assigned to the Zn−O bonding. The latter one is much weak and it is attributed to the carboxyl groups, indicating that the graphene contains small amount of carboxyl groups.[7,8] Figure 4d shows the C1s XPS core level spectrum. The strong binding energy peak at 284.7 eV is assigned to the C—C bonding, 287.8 eV is assigned to the C═O bonding, and the weak binding energy peak at 289.3 eV is assigned to the O—C═O bonding. This result reveals that the graphene in the prepared composite has a very high degree of reduction.[27−29]

Figure 5 shows the UV−vis diffuse reflectance spectra of the prepared ZnO and the graphene−ZnO quasi-shell−core

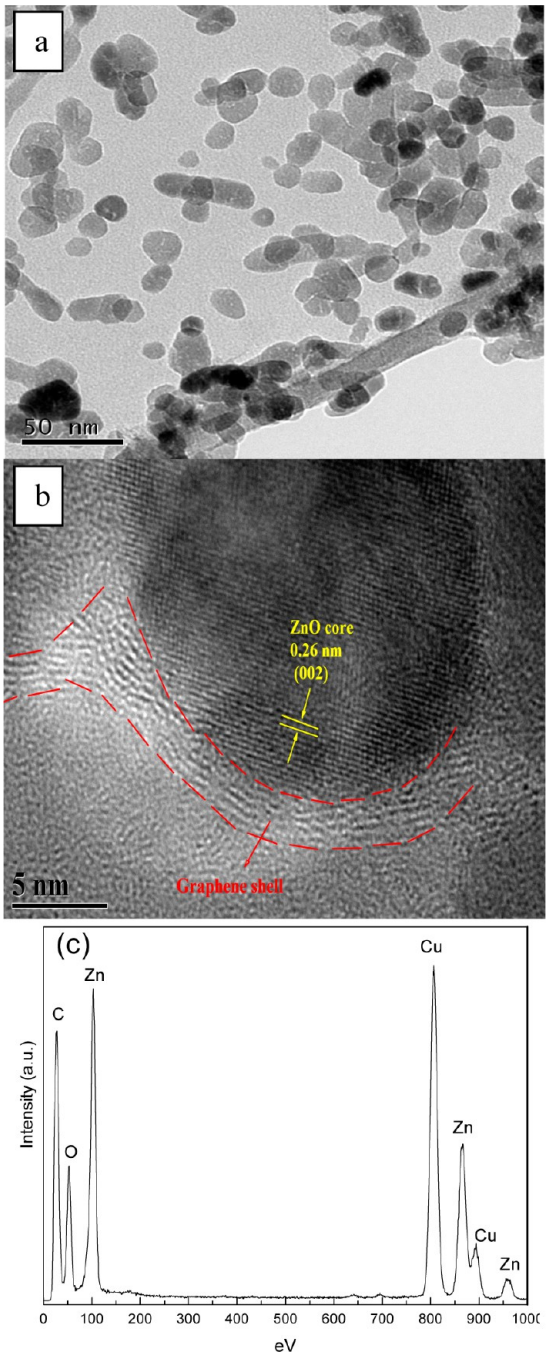

Figure 2. HRTEM morphologies (a, b) and EDS results (c) of the graphene–ZnO quasi-shell–core composite with 10 mg GO addition.

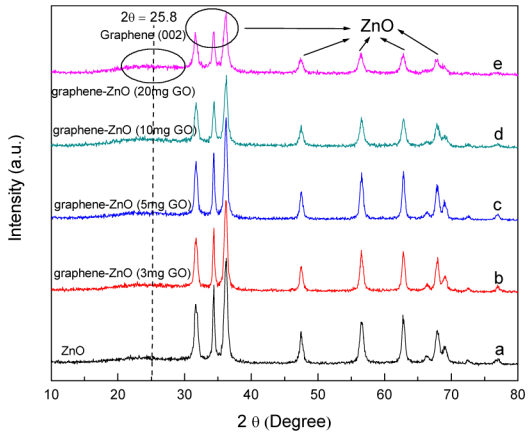

Figure 3. XRD patterns of the graphene–ZnO quasi-shell–core composite with different GO addition: (a) 0; (b) 5; (c) 10; (d) 20; (e) 40 mg.

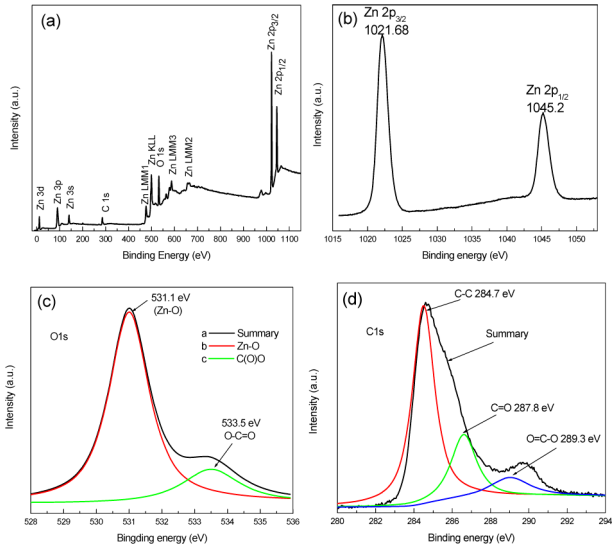

Figure 4. XPS spectra of the graphene–ZnO quasi-shell–core composite with 10 mg GO addition.

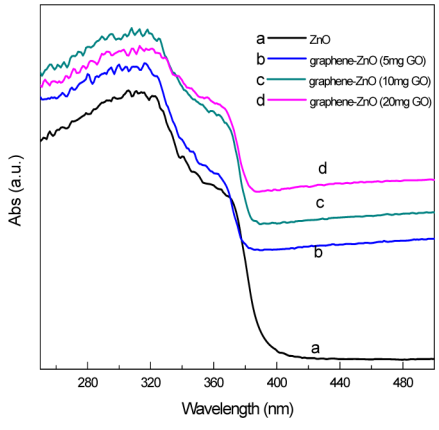

Figure 5. UV–vis diffuse reflectance spectra of the prepared ZnO (a) and the graphene–ZnO quasi-shell–core composites with different GO additions: (b) 5; (c) 10; (d) 20 mg.

composites with different GO additions. When ZnO is coated with graphene, the absorption band-edges of this composite red-shift to >400 nm. The optical absorption intensity increases with the GO addition. These results are in agreement with those reported by Liu et al.[30] The optical absorption at >400 nm of the graphene–ZnO quasi-shell–core composite is mainly provided by the absorption of the graphene with zero bandgap. This absorption cannot change to the energy for the generation of separated electrons and holes, but is simply converted to heat dissipation. In the ultraviolet region (λ < 400 nm), the absorption band-edges of all composites prepared in this study are approximately 380 nm, corresponding to a bandgap of 3.2 eV. In the ultraviolet region, the optical absorption intensity of the graphene–ZnO quasi-shell–core composites is clearly larger than that of ZnO, revealing that

adding GO efficiently improve the photocatalytic performance of ZnO.

Figure 6 shows the RhB degradation curves of the prepared ZnO and graphene−ZnO quasi-shell−core composite with

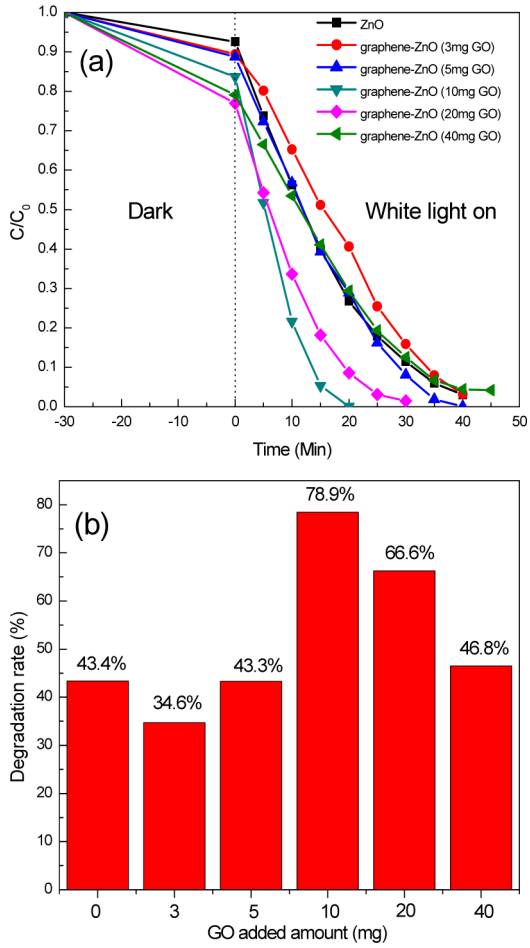

Figure 6. Photocatalytic RhB degradation efficiency (a) and that obtained after 10 min illumination (b) of the prepared ZnO and the grephene-ZnO quasi-shell−core composite with different GO addition.

different GO additions under white light illumination. Before the light was switched on, the photocatalysts were mixed with the RhB under dark condition and stirred for 30 min. According to the data obtained for the 30-min adsorption under dark condition, graphene improves the dye adsorption capacity of ZnO to a certain extent. In order to perform a more intuitive comparison of the prepared series of photocatalysts, 10-min degradation efficiency data under white light illumination was selected and is shown in Figure 6b. The photocatalytic degradation efficiency increases with increasing GO addition and reaches its maximum value when the GO addition is 10 mg (i.e., the optimal photocatalytic degradation efficiency), as shown in Figure 6b. After 10 min of illumination by white light, about 78.9% RhB has already been degraded, exhibiting a high photocatalytic degradation capacity. With a further increase in the GO additions to 20 and 40 mg, the photocatalytic degradation efficiency declines. According to the data shown in Figure 6, the GO addition plays an important role in the photocatalytic degradation performance of the prepared composites. When the GO addition is too low, the graphene is randomly distributed on the ZnO surface and discrete island-like graphene loading forms on the ZnO surface. This discontinuous graphene loading may act as the recombination centers of photogenerated electrons and holes and decrease the photocatalytic degradation efficiency. When the GO addition is too high, a much thicker graphene adhesive layer is formed on the ZnO surface. Because graphene is a black material with 0 eV bandgap, it will absorb a large amount of incident light, thereby reducing the photo absorption of ZnO and thus decreasing the photocatalytic degradation efficiency.

As the results shown in Figure 6a, all of the RhB was degraded by the graphene−ZnO quasi-shell−core composite with 10 mg GO addition after only 20 min of illumination, illustrating its excellent photocatalytic degradation performance. There are plenty of reports concerning about the organic dye degradation using ZnO or graphene-loaded ZnO composites. Xu et al.[7] found that it cost 40 min for the graphene-loaded ZnO composite to degrade the methylene blue under UV light illumination. Li et al.[31] prepared graphene-loaded ZnO composite, and they found that it need 30 min for this composite to degrade all of the RhB under UV light illumination. Li et al.[32] prepared graphene-loaded ZnO composite and found that it cost 40 min for this composite to completely degrade the methylene blue under illumination using a 300 W Xe arc lamp. According to the results obtained from literature mentioned above, the photocatalytic degradation performance of the graphene−ZnO quasi-shell−core composite prepared in the present paper is significantly better than those prepared in the literature. The promotion of the photocatalytic degradation performance of the graphene−ZnO quasi-shell−core composite prepared in the present paper could be attributed to the increase of the contact areas of the graphene and ZnO and, hence, increase the effective area of the interface electric field formed on the interface between the graphene and ZnO, which resulted in the increase of the separation efficiency of the photogenerated electron−hole pairs. The photoinduced electrons and holes generated by ZnO under white light illumination due to its photovoltaic effect. The photogenerated electrons and holes joined the RhB degradation process of the graphene−ZnO quasi-shell−core composite. The photogenerated electrons transferred to the graphene and took part in the reduction reactions of the organic dye occurred on the surface of the graphene. Meanwhile, the photogenerated holes left ZnO and joined the oxidation reactions of the organic dye occurring on ZnO surface.

To further study the separation efficiency of photogenerated electrons and holes, the photoelectrochemical performance of the prepared ZnO and series graphene−ZnO quasi-shell−core photoelectrodes was studied using photoinduced $i-t$ and $i-V$ curves. Figure 7a shows the $i-t$ curves obtained at a 0 V bias potential under white light. The photogenerated current densities decrease gradually during the first three cycles of light switching on and off, possibly due to slight photocorrosion of ZnO in Na_2SO_4 solution under white light. The photogenerated current density of the graphene−ZnO quasi-shell−core composite with 3 mg adding GO is lower than that of ZnO. The photogenerated current density of the prepared composite increases with the increase of the GO addition and reaches the maximum value when the GO addition is 10 mg. With a further increase in GO addition, the photogenerated current density declines. There is a very good corresponding relationship between the photoinduced current densities shown

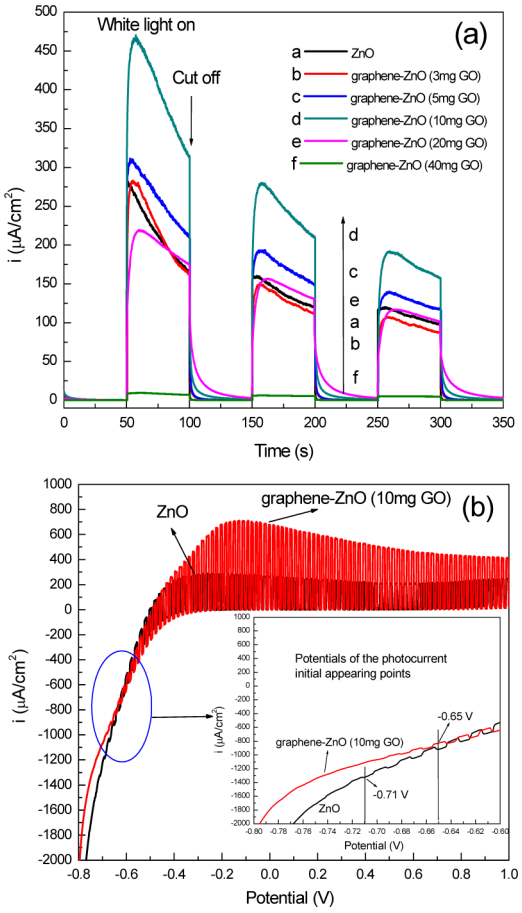

Figure 7. Photoinduced $i-t$ curves (a) and $i-V$ curves (b) of the photoelectrodes prepared by ZnO and graphene−ZnO quasi-shell−core composite with 10 mg GO addition.

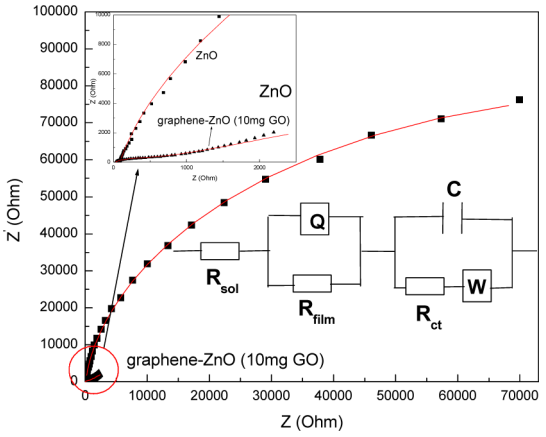

Figure 8. EIS results of the photoelectrodes prepared by ZnO and graphene−ZnO quasi-shell−core composite with 10 mg GO addition and the equivalent circuit for fitting the EIS results obtained in this work.

in Figure 7a, and the photocatalytic RhB degradation results shown in Figure 6.

Figure 7b shows the $i-V$ curves of the prepared ZnO and graphene−ZnO quasi-shell−core composite with 10 mg GO addition. When the bias potential is larger than −0.4 V, the photogenerated current density of the photoelectrode prepared by the graphene−ZnO quasi-shell−core composite with 10 mg addition is much larger than that of the photoelectrode prepared by ZnO. When the bias potential increases above −0.2 V, the photogenerated current density of the photoelectrode prepared by the graphene−ZnO quasi-shell−core composite with 10 mg adding GO is approximately two times greater than that of the photoelectrode prepared by ZnO. As we may know, the threshold bias potential for generating current in a semiconductor under light illumination is approximately equal to its Fermi level potential.[33] As shown in Figure 7b, the threshold bias potential for generating current in ZnO under white light illumination is −0.71 V, and this value positively shifts to −0.65 V after covering with graphene. This result reveals that the graphene loading causes a positve shift of the Fermi level of ZnO, thus causing the energy band of ZnO to bend. An effective interfacial electric field will form between ZnO and graphene, effectively enhancing the separation efficiency of photogenerated electron−hole pairs and improving its photoelectrochemical and photocatalytic performance.

Figure 8 shows the electrochemical impedance spectroscopy (EIS) results of the photoelectrodes prepared by ZnO and graphene−ZnO quasi-shell−core composite with 10 mg GO addition in 0.1 M Na_2SO_4 solution under dark condition. The AC impedance of the photoelectrode is mainly decided by the solution resistance, the migration resistance of the photogenerated electrons in the material and interfacial reaction resistance. Therefore, EIS can be used to study the migration ability of the photogenerated electrons and the interface reaction ability of the electrons in the graphene−ZnO composite materials. The EIS results were fitted by the equivalent circuit inserted in Figure 8. In this equivalent circuit, R_{sol} was the solution resistance; R_{film} was the migration resistance of the charge carriers in the thin-film photoelectrode; Q was constant phase angle element. Its impedance was equal to $(Y_0(j\omega)^n)^{-1}$, where ω was the ac-voltage angular frequency (rad s^{-1}), and Y_0 and n were the frequency-independent parameters; R_{ct}, C, and W were used to describe the behaviours of the photogenerated electrons and holes on the interface between the semiconductor material and the electrolyte. R_{ct}, C, and W were the electron transfer resistance on the interface, the interface capacitance, and the Warburg resistance caused by the diffusion effect of the electrolyte, respectively. As showed in Figure 8, the measured data are the dots with different symbols, while the fitted results are the solid lines. The measured data are fitted very well. Table 1 shows the parameters of the EIS data. The R_{film} value of ZnO thin film was 6304 Ω cm^2, while this value of graphene coated ZnO thin film decreased to 336.2 Ω cm^2, which is decreased by about 20 times of that of ZnO. This result indicated that the continuous electron transfer path was established through the coated graphene on the surface of ZnO. Therefore, the electron migration resistance within the thin film could be dramatically reduced, which resulted in the effectively avoiding of the recombination of the photogenerated electrons and holes. ZnO, acting as an electron acceptor, had been widely used in the field of dye-sensitized or narrow bandgap semiconductor quantum dot sensitized solar cell. However, the prepared graphene−ZnO quasi-shell−core materials in this work could greatly enhance the electron mobility of ZnO. Therefore, this composite material would have a great potential application in the field of solar cells. The R_{ct} value obtained for ZnO was 1.213×10^5 Ω cm^2 (Table 1). After being coated with graphene, the R_{ct} value decreased to 332.7 Ω cm^2, which is three orders of magnitude lesser than the material without graphene. The decrease of the R_{ct} value

dx.doi.org/10.1021/am403149g | ACS Appl. Mater. Interfaces 2013, 5, 12361−12368

Table 1. Fitted Parameters of the EIS Results of the Photoelectrodes Prepared by ZnO and Graphene−ZnO Quasi-Shell−Core Composite with 10 mg GO Addition in 0.1 M Na_2SO_4 Solution under Dark Conditions

sample	R_{sol} (Ω cm^2)	R_{film} (Ω cm^2)	Q (Ω^{-1} cm^{-2} s^n)	n	C (μF cm^{-2})	R_{ct} (Ω cm^2)	W_{ss} (Ω cm^2)
ZnO	81.38	6304	6.514×10^{-5}	0.8388	1.083×10^{-5}	1.213×10^{5}	3.819×10^{-5}
graphene + ZnO (10 mg GO)	75.03	336.2	2.063×10^{-5}	0.8849	3.775×10^{-5}	332.7	4.25×10^{-4}

indicated that the graphene loading significantly improved the interfacial electron transfer velocity and lower down the interfacial reaction resistance. The reasons for causing this phenomena, on the one hand, may be due to the formation of the interfacial electric field between the interface of graphene and ZnO, which improved the separation efficiency of the photogenerated electrons and holes and made the interfacial reaction much easier, on the other hand, may be due to the lowering down of the interface electrochemical reaction energy barrier by the coated graphene and hence resulted in the decrease of the interfacial reaction resistance.

As the results shown in Figure 7a, the photogenerated current densities decrease with increasing cycles of white light switching on and off, indicating the existence of corrosion of ZnO during the photoelectrochemical reactions in a Na_2SO_4 solution.[34] If this corrosion phenomenon exists in the photocatalytic degradation of organic dye, it is bound to negatively affect the feasibility of this composite material in the field of photocatalysis. In order to investigate the stability of the graphene−ZnO quasi-shell−core materials in the process of photocatalysis, five successive cyclic RhB degradation tests were performed and the relevant experimental results are shown in Figure 9. From the results shown in Figure 9, the photocatalytic

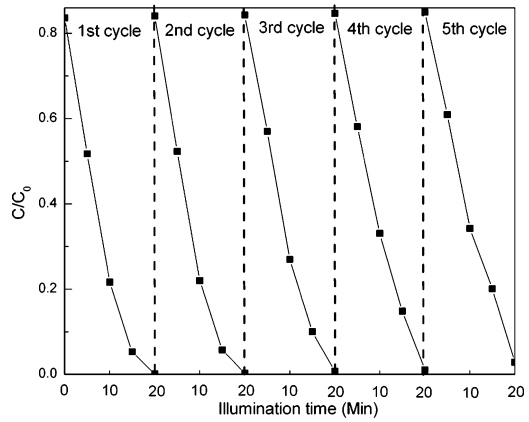

Figure 9. Stability study for the photocatalytic RhB degradation by the prepared graphene−ZnO quasi-shell−core composite with 10 mg GO addition.

RhB degradation efficiency of this composite material does not show noticeable decline after five successive cyclic RhB degradation tests, indicating that there is no serious corrosion of ZnO during the process of photocatalytic degradation. The existence of the ZnO corrosion in the $i-t$ curves in Figure 7a may be due to the separation of photoelectrochemical reactions. In the $i-t$ curve test, the reduction process of photogenerated electrons occurs on the surface of the counter electrode, while the oxidation process of photogenerated holes occurs on the surface of the ZnO photoelectrode. On the surface of the ZnO photoelectrode, the photogenerated holes are captured by the OH^-, ionized by H_2O. With consumption of OH^-, H^+ will enrich on the surface of the ZnO photoelectrode and cause a decrease in the pH value of the local electrolyte near the ZnO photoelectrode, leading to the occurrence of ZnO corrosion during the $i-t$ measurements. However, in the photocatalytic RhB degradation process, the redox reactions of photogenerated electrons and holes occur on the surfaces of the catalysts. The H^+ products from the oxidation reactions of the photogenerated holes can rapidly neutralize the OH^- product from the reduction reactions of the photogenerated electrons. Therefore, the corrosion of ZnO is effectively avoided during the photocatalytic RhB degradation process, and the stability of the graphene−ZnO quasi-shell−core materials in the process of photocatalysis is significantly improved.

Figure 10 schematically shows the proposed mechanism for the improvement of the photoelectrochemical performance and

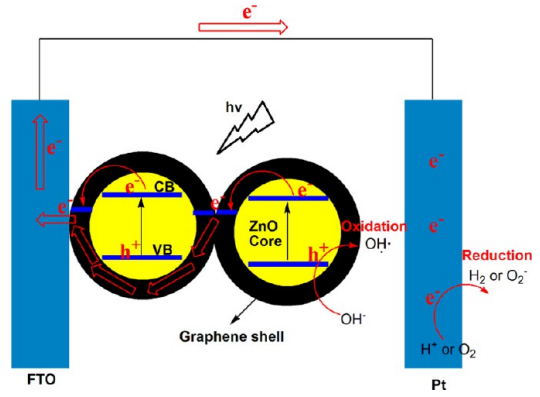

Figure 10. Proposed mechanism for the improvement of the photoelectrochemical and photocatalytic performance of the graphene−ZnO quasi-shell−core composite material.

photocatalytic properties of the graphene−ZnO quasi-shell−core material. Because the graphene is coated onto the surface of ZnO nanoparticles, continuous conductive paths are built through the graphene particles, thereby effectively reducing the transfer resistance of photogenerated electrons and inhibiting the recombination of photogenerated electrons and holes. Furthermore, because the Fermi level of graphene is more positive than that of ZnO, the Fermi level of ZnO will shift in a positive direction when graphene coats on its surface. An interfacial electric field will form due to the exchange of electrons at the interface between graphene and ZnO. The formation of this electric field can further improve the separation efficiency of photoinduced electron−hole pairs. When photogenerated electrons migrate to the FTO conductive glass and finally are transferred to the counter electrode, they participate in the reduction reactions on the counter electrode surface, and the holes left on the VB of ZnO will react with OH^- and generate $OH^\bullet$ or participate in the RhB dye degradation process. If the graphene−ZnO quasi-shell−core material is further loaded with p-type dye or p-type semiconductor quantum dots with narrow bandgap, a p−n heterojunction electric field will form on the interface between

them. This electric field will significantly improve the separation efficiency of photogenerated electron−hole pairs. Meanwhile, the graphene possesses very high efficient electron transfer ability. This high electron transfer ability improves the lifetime of photoinduced electrons and holes. This indicates that it has great application potential and this potential should be explored in detail.

4. CONCLUSIONS

In this study, the graphene−ZnO composite with quasi-shell−core structure was successfully prepared using a one-step wet chemical method. Coating ZnO with graphene significantly improves the photocatalytic RhB degradation property and the photoelectrochemical performance. The graphene−ZnO quasi-shell−core composite with 10 mg GO addition possesses optimal photocatalytic degradation efficiency. After 10 min of illumination by white light, about 78.9% RhB already degrades, and complete degradation is achieved after only 20 min. According to the results from the photoinduced $i-t$ and $i-V$ curves, ZnO coating with the appropriate amount of graphene can significantly improve its photogenerated current density and the graphene−ZnO composite achieves the highest photoinduced current density when the added GO amount is 10 mg. This is in agreement with the GO amount that produces the best photocatalytic degradation property in graphene−ZnO composites. The improvement in photoelectrochemical performance and photocatalytic dye degradation capability are caused by the establishment of an effective electric field between ZnO and the graphene coating layer and the dramatic decrease in migration resistance of the photogenerated electrons due to the graphene coating layer on the ZnO surface.

AUTHOR INFORMATION

Corresponding Author

*E-mail: zychen@qdio.ac.cn. Tel.: +86 532 8289 8731. Fax: +86 532 8288 0498.

Author Contributions

All authors contributed equally.

Notes

The authors declare no competing financial interest.

ACKNOWLEDGMENTS

This work was financially supported by the Hundreds-Talent Program of the Chinese Academy of Sciences (Y02616101L).

REFERENCES

(1) Xiang, Q. J.; Yu, J. G.; Jaroniec, M. *Chem. Soc. Rev.* **2012**, *41*, 782−796.
(2) Xiang, Q. J.; Yu, J. *J. Phys. Chem. Lett.* **2013**, *4*, 753−759.
(3) Kamat, P. V. *J. Phys. Chem. Lett.* **2011**, *2*, 242−251.
(4) Liang, Y.; Wang, H.; Casalongue, H. S.; Chen, Z.; Dai, H. *Nano Res.* **2010**, *3*, 701−705.
(5) Zhang, X. Y.; Li, H. P.; Cui, X. L.; Lin, Y. *J. Mater. Chem.* **2010**, *20*, 2801−2806.
(6) Zhu, C.; Guo, S.; Wang, P.; Xing, L.; Fang, Y.; Zhai, Y.; Dong, S. *Chem. Commun.* **2010**, *46*, 7148−7150.
(7) Xu, T.; Zhang, L.; Cheng, H.; Zhu, Y. *App. Catal. B: Environ.* **2011**, *101*, 382−387.
(8) Chang, H.; Sun, Z.; Ho, K.Y. F.; Tao, X.; Yan, F.; Kwok, W. M.; Zheng, Z. *Nanoscale* **2011**, *3*, 258−264.
(9) Yu, J.; Zhang, J.; Jaroniec, M. *Green Chem.* **2010**, *12*, 1611−1614.
(10) Cao, A.; Liu, Z.; Chu, S.; Wu, M.; Ye, Z.; Gai, Z.; Chang, Y.; Wang, S.; Gong, Q.; Liu, Y. *Adv. Mater.* **2010**, *22*, 103−106.
(11) Ng, Y. H.; Iwase, A.; Kudo, A.; Amal, R. *J. Phys. Chem. Lett.* **2010**, *1*, 2607−2612.
(12) Iwase, A.; Ng, Y. H.; Ishiguro, Y.; Kudo, A.; Amal, R. *J. Am. Chem. Soc.* **2011**, *133*, 11054−11057.
(13) Fu, Y.; Wang, X. *Ind. Eng. Chem. Res.* **2011**, *50*, 7210−7218.
(14) Kim, H.; Moon, G.; Monllor-Satoca, D.; Park, Y.; Choi, W. *J.Phys. Chem. C* **2012**, *116*, 1535−1543.
(15) Emin, S.; Fanetti, M.; Abdi, F. F.; Lisjak, D.; Valant, M.; Krol, V. D. R.; Dam, B. *ACS Appl. Mater. Interfaces* **2013**, *5*, 1113−1121.
(16) Jiang, W. T.; Wu, C. T.; Sung, Y. H.; Wu, J. J. *ACS Appl. Mater. Interfaces* **2013**, *5*, 911−917.
(17) Maeda, K.; Takata, T.; Hara, M.; Saito, N.; Inoue, Y.; Kobayashi, H.; Komen, K. *J. Am. Chem. Soc.* **2005**, *127*, 8286−8287.
(18) Wolcott, A.; Smith, W. A.; Kuykendall, T. R.; Zhao, Y.; Zhang, J. Z. *Adv. Fun. Mater.* **2009**, *19*, 1849−1856.
(19) Yang, X.; Wolcott, A.; Wang, G.; Sobo, A.; Fitzmorris, R. C.; Qian, F.; Zhang, J. Z.; Li, Y. *Nano Lett.* **2009**, *9*, 2331−2336.
(20) Yang, J. L.; An, S. J.; Park, W. I.; Yi, G. C.; Choi, W. *Adv. Mater.* **2004**, *16*, 1661−1664.
(21) Elmolla, E. S.; Chaudhuri, M. *J. Hazar. Mater.* **2011**, *173*, 445−449.
(22) Qin, H.; Li, W.; Xia, Y.; He, T. *ACS Appl. Mater. Interfaces* **2011**, *3*, 3152−3156.
(23) Parida, K. M.; Parija, S. *Sol. Energy* **2006**, *80*, 1048.
(24) Parida, K. M.; Dash, S. S.; Das, D. P. *J. Coll. Inter. Sci.* **2006**, *98*, 787.
(25) Seager, C. H.; Warren, W. L.; Tallant, D. R.; Voigt, J. A. *Appl. Phys. Lett.* **1996**, *68*, 403−405.
(26) Son, D. I.; Kwon, B. W.; Park, D. H.; Seo, W. S.; Yi, Y.; Angadi, B.; Lee, C. L.; Choi, W. K. *Nat. Nanotech.* **2012**, *7*, 465−471.
(27) Hummers, W. S.; Offeman, R. E. *J. Am. Chem. Soc.* **1958**, *80*, 1339.
(28) Zhang, H.; Fan, X.; Quan, X.; Chen, S.; Yu, H. *Environ. Sci. Technol.* **2011**, *45*, 5731−5736.
(29) Wen, Y.; Ding, H.; Shan, Y. *Nanoscale* **2011**, *3*, 4411−4417.
(30) Liu, S.; Liu, C.; Wang, W.; Cheng, B.; Yu, J. *Nanoscale* **2012**, *4*, 3193−3200.
(31) Li, B.; Cao, H. *J. Mater. Chem.* **2011**, *21*, 3346−3349.
(32) Li, B.; Liu, T.; Wang, Y.; Wang, Z. J. *Colloid Interface Sci.* **2012**, *377*, 114−121.
(33) Long, M.; Cai, W.; Kisch, H. *J. Phys. Chem. C* **2008**, *112*, 548−554.
(34) Zhang, L.; Cheng, H.; Zong, R.; Zhu, Y. *J. Phys. Chem. C* **2009**, *113*, 2368−2374.